Performance of the vertical optical filter for the NG-3 30 m SANS instrument at the National Institute of Standards and Technology's Center for Neutron Research

Jeremy C. Cook[a)]
Department of Materials Science and Engineering, University of Maryland, College Park, Maryland 20742-2115 and NIST Center for Neutron Research, National Institute of Standards and Technology, 100 Bureau Drive, Stop 8563, Gaithersburg, Maryland 20899-8563

Charles J. Glinka and Ivan G. Schröder
NIST Center for Neutron Research, National Institute of Standards and Technology, 100 Bureau Drive, Stop 8563, Gaithersburg, Maryland 20899-8563

(Received 27 July 2004; accepted 20 October 2004; published online 20 January 2005)

The straight neutron guide and crystal filter formerly used to supply a cold neutron beam to the NG-3 30 m small angle scattering instrument at the National Institute of Standards and Technology Center for Neutron Research has been replaced by a vertically-kinked "optical filter" neutron guide that eliminates direct lines-of-sight between the instrument and the neutron source. Due to pre-existing lateral spatial constraints, the optical filter bend is in a vertical plane requiring a vertical displacement of the sample-detector axis by about 14 cm. The optical filter is successful in excluding unwanted fast neutrons and gamma rays from the beam at the sample position without the use of crystal filters. We show that the optical filter provides neutron current density gains at the sample by a factor of about 1.8 at 15 Å neutron wavelength with negligible increase in the beam divergence, whilst allowing some measurement capability at wavelengths shorter than 4 Å (previously excluded by the beryllium–bismuth crystal filter). © *2005 American Institute of Physics.* [DOI: 10.1063/1.1844472]

I. INTRODUCTION

The indispensability of neutron guide tubes for the efficient transport of cold neutron beams over large distances has been recognized since the pioneering days of the technique.[1] Straight neutron guides are relatively simple to construct and align and provide approximately spatially-uniform neutron beams at all wavelengths. Straight guides have some natural beam filtering ability. If one considers the case that they have perfect reflectivity, are fully illuminated, and have small solid angles for lines-of-sight from the source to the exit, their neutron transmission increases approximately proportional to the neutron wavelength squared. Thus there is a natural bias against short wavelength neutron transmission, whilst the fast neutrons and gamma rays, the majority of which do not "see" the boundaries of the guide, tend to decrease approximately inversely proportional to the square of the distance from the source. However, the natural filtering ability of a straight guide is often insufficient over the distances considered without additional fast neutron and gamma ray removal from the beam. On the straight neutron guides that view the cold neutron source at the National Institute of Standards and Technology Center for Neutron Research (NCNR), this task is often performed by a crystal filter. Up until March 2002, a straight guide-crystal filter arrangement was used for the "30 m" small angle neutron scattering (SANS) instrument installed on the cold neutron guide NG-3 as illustrated schematically in Fig. 1.

The NG-3 crystal filter consisted of 8 in. each (in the beam direction) of vacuum-cast beryllium and quasisingle crystal bismuth. The crystals were contained in a cryostat and cooled by liquid nitrogen in order to reduce thermal diffuse scattering of the desirable cold neutrons. At these thicknesses, polycrystalline beryllium is an efficient scatterer of neutrons with wavelengths shorter than 4 Å (the Bragg scattering threshold), whilst the main role of the bismuth is to efficiently attenuate gamma rays in the beam without significantly attenuating the neutrons in the transmission band of the beryllium. Relatively large grained vacuum-cast beryllium was chosen over the more traditional hot-pressed, finely powdered beryllium because it produces about one-half of the beam broadening of the latter due to small angle scattering.[2] Having single crystal or quasisingle crystal, as opposed to polycrystalline bismuth, increases the neutron transmission in the 4–6.5 Å wavelength range (between the Bragg scattering thresholds of Be and Bi). The transmission properties of these crystals are further discussed, for example, in Refs. 3–6, and associated references.

There are several obvious disadvantages of using the straight guide-crystal filter arrangement: (i) The guide sections feeding the SANS instrument clearly do not exploit the full height of the preceding ^{58}Ni-coated guide. (ii) The maximum transmission of the cooled filter for neutrons in the transmission band is only about 72% near $\lambda = 4$ Å falling to

a)Author to whom correspondence should be addressed; electronic mail: jeremy.cook@nist.gov

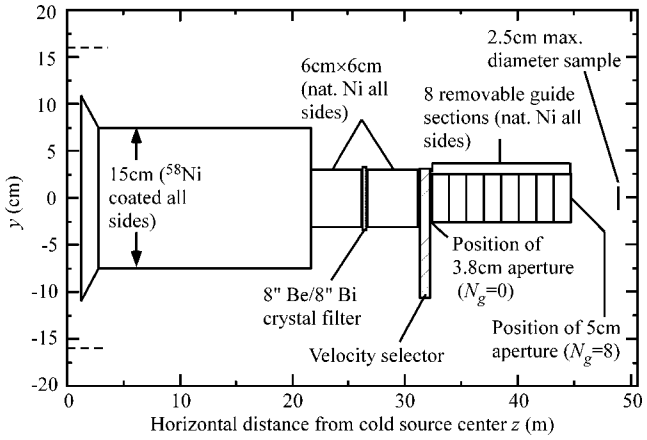

FIG. 1. Pre-March 2002 configuration of the NG-3 neutron guide tube (side view) for the 30 m SANS instrument (note different y and z scales). z represents the distance along the beam direction from the center of the cold source. Unable to exploit the divergence of the initial more than 20 m of ^{58}Ni-coated guide, the SANS instrument uses guides coated on all sides with natural Ni within about 27 m of the sample position. The guide cut required to accommodate the crystal filter cryostat is a little over 0.5 m long and the minimum gap between the guides on each side of the velocity selector is a little over 1.2 m. When all 8 removable guides are inserted (N_g=8) as shown, a circular source aperture (typically 5 cm diameter) is inserted just downstream of the final removable guide section. When all 8 guides are removed (N_g=0), typically a 3.8 cm diameter source aperture is placed at the downstream end of the velocity selector gap. The dashed lines indicate the diameter of the spherical, first-generation liquid hydrogen cold source (not shown explicitly).

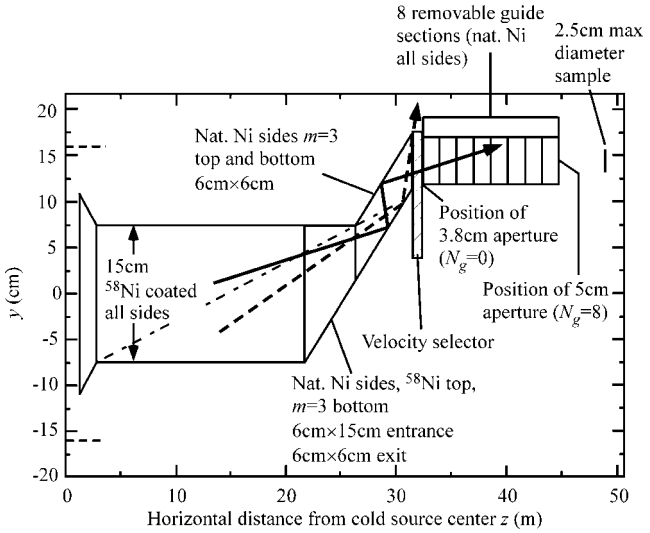

FIG. 2. Post-March 2002 configuration of the NG-3 neutron guide tube (side view) for the 30 m SANS instrument (note different y and z scales). The configuration is shown with all 8 removable guides inserted in the beam (N_g=8). The OF (optical filter) is illuminated by the full area of the preceding 6 cm×15 cm ^{58}Ni guide. The vertical displacement of the beam center at the sample is approximately 14.3 cm which is just sufficient to exclude a line-of-sight between the source and the exit of the filter (see dotted–dashed line). The solid arrowed line illustrates a trajectory undergoing an even number of reflections (2) from the upward-sloping surfaces of the OF, emerging with the same y-z plane projection angle with which it entered. Such trajectories can potentially be transmitted towards the sample either directly or by further reflections in the removable guide sections. The dashed-arrowed line illustrates a trajectory that is once-reflected from the upward-sloping surfaces of the OF and emerges at an inappropriate angle to be transmitted further. (Note that the angles are greatly exaggerated by the different y and z scales.) The horizontal dashed lines indicate the diameter of the spherical, first-generation liquid hydrogen cold source.

less than 56% at $\lambda = 15$ Å. (iii) The length of the filter cryostat requires a guide cut exceeding 0.5 m, resulting in neutron beam divergence losses that are particularly costly at long wavelengths. (iv) The losses in (iii) are further enhanced by small angle scattering in the crystal. (v) Periodic maintenance (liquid nitrogen filling and insulation vacuum pumping) of the filter cooling system is required. In light of these disadvantages, we undertook a study of an alternative "optical filter" guide (a term first employed, we believe, by Hayter[7]) to replace the approximately 9.5 m section of NG-3 comprising the two 4.5 m long, 6 cm×6 cm sections of guide each side of the crystal filter, the filter itself, and its associated guide gap. Henceforth we refer to this 9.5 m section as the "filter section" of the guide. Optical filters are already in use at the NCNR on the Disk Chopper Spectrometer[8] and on the neutron spin echo spectrometer. An optical filter is a neutron guide that delivers a beam that has fairly uniform spatial and angular neutron distributions similar to that of a straight guide but uses a bend or kink to exclude direct lines-of-sight between the source and the beam exit. [We point out that polygonal approximations to curved guides with no line-of-sight, although also acting as slow neutron band pass filters, are conventionally *not* referred to as optical filters because their spatial beam distributions are skewed by garland reflections (see Ref. 12).] As with any such guide, the optical filter exhibits the familiar short-wavelength transmission "cutoff" that is characteristic of the minimum bend angle and the neutron reflective coatings used on it. Most of the unwanted short wavelength neutrons and source (core) gamma rays cannot negotiate the bend and are transmitted through the reflecting surface into a region where they can be absorbed. In most neutron guides that are exposed to moderate neutron fluxes, the majority of these neutrons are captured within the boron-containing glass that constitutes the substrate for the neutron reflecting layers. The quasi-isotropic prompt gammas resulting from this capture are low in energy (478 keV) and are easy to shield from personnel and sensitive equipment. Their intensity in the final beam direction is usually tolerable from the sample point of view. The typically smaller fraction of faster neutrons that are not appreciably absorbed in the glass may be captured in fast neutron shielding, if necessary. Likewise, the core gamma rays can be captured in appropriate gamma ray shielding. By dissipating most of the unwanted radiation far from the final beam delivery point, instrumental background levels are kept low. Transmission properties of neutron optical filters have been further discussed in Ref. 9.

The principal constraints on the optical filter design were as follows: (i) The original approximately 20 m of guide would remain in place. (ii) The location of the "footprints" of the velocity selector, the 5 cm×5 cm removable guide sections, and the detector tank would remain unchanged. Only a vertical displacement of these elements would be permitted. (iii) The divergence of the beam at the sample should not increase. (iv) Direct lines of sight must be eliminated.

In order to satisfy these constraints, we proposed a vertically-oriented "double kink" optical filter design that necessitates the raising of the velocity selector-sample-detector

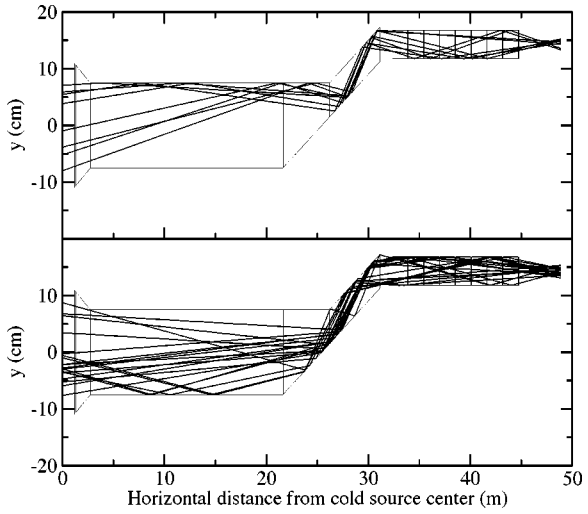

FIG. 3. *y-z* projections of a few Monte Carlo simulated trajectories that successfully arrive at a 2.5 cm diameter sample (represented by the vertical bar at the extreme right). The upper plot shows trajectories that made their first reflection on an upper surface of the guide and the lower plot shows trajectories that made their first reflection on a lower surface. Note that the different *y* and *z* scales in this projection both greatly exaggerate and distort the reflection angles such that reflections from the sloping surfaces appear to be nonspecular.

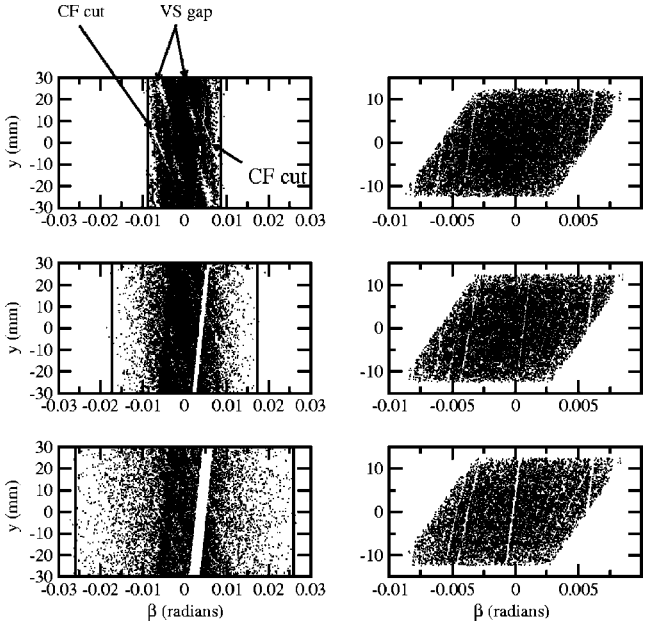

FIG. 4. CF (crystal filter) configuration: Entrance acceptance diagrams (left-hand column) for neutrons entering the CF filter section (with $N_g=8$) that arrive at the 2.5 cm diameter sample, and phase space diagrams (right-hand column) of the same neutrons at the sample for monochromatic wavelengths (top to bottom) $\lambda=5$ Å, 10 Å, and 15 Å. These diagrams refer to the vertical displacement and the vertical component, β, of the polar angle with respect to the *z*-axis only. Many of the blank stripes running bottom left-to-top right are due to the effects of gravity. The two pairs of prominent blank stripes sloping top left to bottom right are due to the velocity selector (VS) gap and the CF guide cut, as indicated.

plane (see Fig. 2). For brevity, henceforth we refer to the optical filter and the original crystal filter configurations of the guide as the "OF" and "CF" configurations, respectively.

The OF relies on transmitting neutrons undergoing even numbers of reflections from the upward-sloping parallel surfaces such that every second reflection restores the initial neutron trajectory orientation, but with a vertical displacement, rather like a periscope. In this way we are able to achieve a horizontally-oriented beam with similar divergence characteristics at the sample as was obtained with the previous straight guide-crystal filter arrangement. This is illustrated in Fig. 3 by tracing the *y-z* projection of a few of the simulated trajectories that successfully reach the sample for a neutron wavelength of 15 Å. In this case, the sample is a 25 mm diameter disk placed concentrically with the beam exit from the guide. For clarity, the upper plot in Fig. 3 illustrates trajectories that made their first reflection on an upper surface of the guide and the lower plot illustrates trajectories making their first reflection on a lower surface. Those neutrons undergoing an odd number of reflections from the vertically sloping surfaces emerge along a vertically-canted axis and are largely rejected from the beam delivered to the sample. This is illustrated by the dashed-arrowed line in Fig. 2. These rotated-axis neutrons can either be absorbed or conceivably used in an application aligned along the rotated-axis.

II. POSSIBILITIES FOR NEUTRON INTENSITY AND MEASURING RANGE ENHANCEMENTS USING THE OPTICAL FILTER

Because the delivered beam divergence must not increase, beam current density gains at the sample cannot be achieved by net focusing of the beam. A remaining optical possibility for achieving such gains is for the OF to better exploit the full height of the preceding (15 cm $\times$ 6 cm) beam, recognizing that the CF arrangement views only the 6 cm $\times$ 6 cm central portion of it. The "optical" aspects of the performance of the CF and OF guide configurations are well illustrated by considering both the acceptance diagrams[10–14] for neutrons entering the filter section that arrive at the sample and the final phase-space diagram of those same neutrons at the sample. The horizontal plane acceptance of the CF and OF configurations are approximately equivalent because identical coatings and guide widths are used, apart from the fact that the OF benefits from having neutron reflective surfaces in place of the guide cut previously occupied by the filter cryostat. Therefore, we consider only the vertical acceptance (*y-z* plane projection).

Figures 4 and 5 show Monte Carlo-generated acceptance diagrams for the CF and OF arrangements respectively (calculated for all eight removable guides inserted in the beam $[N_g=8]$ as shown in Figs. 1 and 2. In both figures, the left-hand column depicts the region of phase space occupied by neutrons entering the filter sections that successfully arrive at the sample. The right-hand column shows the phase-space distribution of the same neutrons at the sample. As in Fig. 3, the sample is a 2.5 cm diameter disk placed concentrically with the beam exit (hence the vertical boundaries of the phase-space diagram at $y=\pm 1.25$ cm). The three rows from top to bottom are simulations for $\lambda=5$ Å, 10 Å, and 15 Å, respectively, using the reflectivity models described later in this article. The vertical bold lines in Fig. 4 correspond to the critical angle for natural nickel. In most cases, the blank

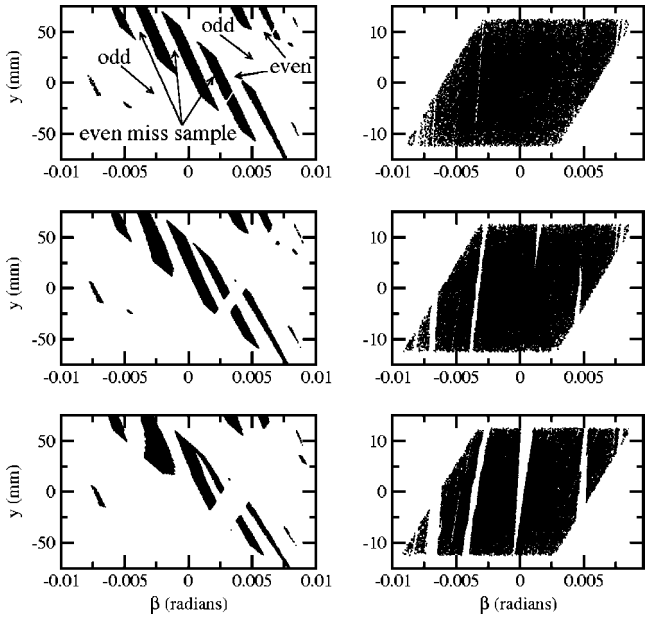

FIG. 5. OF (optical filter) configuration: Entrance acceptance diagrams (left-hand column) for neutrons entering the OF filter section that arrive at the 2.5 cm diameter sample and phase-space diagrams (right-hand column) of the same neutrons at the sample for monochromatic wavelengths (top to bottom) $\lambda = 5$ Å, 10 Å, and 15 Å. These diagrams refer to the vertical displacement and the vertical component, β, of the polar angle with respect to the z-axis only. Many of the blank stripes running bottom left-to-top right are due to the effects of gravity. The wide blank stripes (labeled "odd") running in the opposite sense in the left-hand column are mainly due to losses of neutrons undergoing odd numbers of reflections from the vertically-sloping surfaces that cannot reach the sample. These missing neutrons emerge around a vertically-canted axis and, in the case of NG-3, are absorbed in the velocity selector and surrounding shielding. The narrower, steeper stripes (labeled "even miss sample") dividing the main transmission regions in the left-hand column are mainly due to neutrons that are able to reach the guide exit but pass by the sample.

regions canted bottom left-to-top right are due to gravitational effects that are included more or less rigorously in the simulations. In the left-hand column of Fig. 4, the decreasing point density at higher y-z plane-projected angle magnitude, $|\beta|$, is consistent with the decreasing visibility of the top and bottom reflecting surfaces of the prefilter guide as the step in guide height is approached (the maximum $|\beta|$ of an unreflected neutron at the entrance to the filter section is 0.0056 rad). The very low density of points outside of the solid lines indicates that the acceptance at the sample is largely determined by the critical angle of the natural nickel-coated guide sections downstream of the filter section entrance.

The very different entrance acceptance diagram for the OF in Fig. 5 shows that the full height of the illuminating guide participates. The broad blank regions canted bottom right-to-top left, separating three distinct and similarly angled bands of transmitted intensity, are mainly due to phase space regions that favor odd numbers of reflections from the upward-sloping surfaces of the OF. Such trajectories are absent from the beam at the guide exit and at the sample. Not all of the trajectories undergoing even numbers of reflections from the upward-sloping surfaces of the OF reach the sample since it is both of smaller area than the guide exit and displaced from it. This is the origin of most of

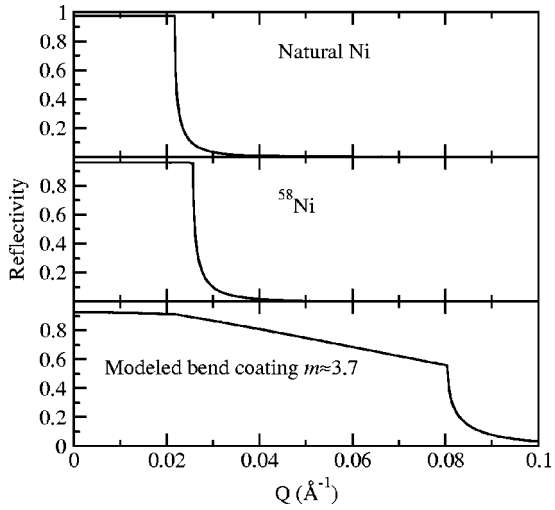

FIG. 6. Model reflectivities used in the Monte Carlo simulations.

the narrower blank "stripes," canted more steeply top left to bottom right, that divide the otherwise transmitting regions.

Figure 5 demonstrates that the final beam divergence at the sample is similar to that of the CF and that the OF produces a beam at the sample that has a reasonable degree of spatial uniformity. As was the case in Fig. 4, most of the blank stripes canted bottom left-to-top right that increase in width with increasing wavelength are due to the influence of gravity. Gravity is also responsible for the curvature of the boundaries between some of the transmitting and nontransmitting regions that becomes more exaggerated with increasing wavelength.

III. SIMULATIONS AND MEASUREMENTS

The simulations were Monte Carlo ray-tracing with partial corrections due to gravitational effects. The simulation models assume no misalignments of the guide elements from their intended positions. The types of reflective coatings used on each major section of guide are indicated in Figs. 1 and 2 for the CF and OF configurations of NG-3 respectively, noting that only the elements occupying the filter section have been replaced.

Initial simulations were performed for configurations of the CF arrangement for which measured data exist, using the modeled geometry and brightness of the first-generation (pre-March 2002) liquid hydrogen cold source (CS-I). The guide up to the point immediately preceding the crystal filter had been previously modeled using the natural Ni and ^{58}Ni reflectivities shown in Fig. 6. These reflectivities are plotted as a function of wave vector transfer magnitude, Q, which is given by

$$Q = \frac{4\pi}{\lambda} \sin\theta \approx \frac{4\pi\theta(\text{rads})}{\lambda}, \tag{1.1}$$

where θ is the scattering angle and the small angle approximation indicated nearly always applies.

The simulated capture flux at this position of $1.76(2) \times 10^9$ cm^{-2} s^{-1} (where the indicated error is statistical) compares well with a measured capture flux[15] of $1.70(4) \times 10^9$ cm^{-2} s^{-1} (where the indicated error is mainly due to

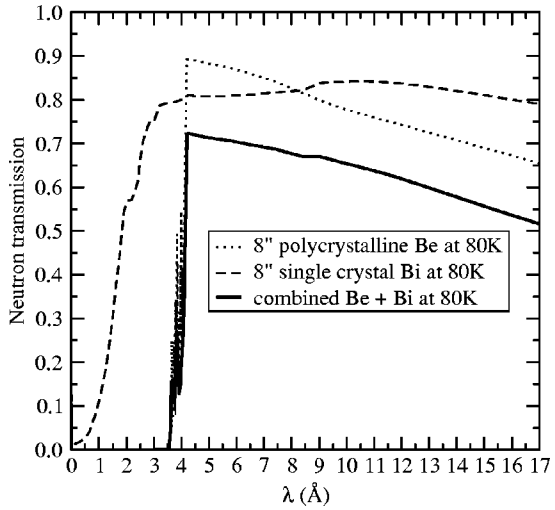

FIG. 7. The modeled transmission of the 8 in. beryllium–8 in. bismuth filter at 80 K used in the Monte Carlo simulations. The dotted line is the calculated transmission for 600 μm grain size beryllium, the dashed line is the calculated transmission for single crystal bismuth, and the solid line is the product of the separate transmissions representing the combined transmission.

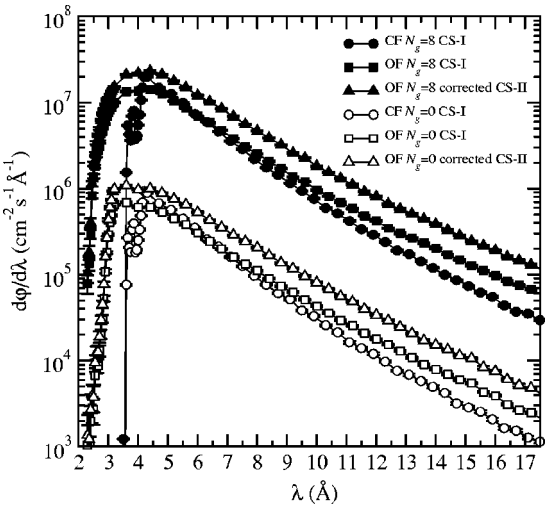

FIG. 8. Simulated values of $d\varphi/d\lambda$ for the CF (crystal filter) and OF (optical filter) configurations of NG-3 assuming CS-I (original source) brightness and geometry. The data labeled "corrected CS-II" (upgraded source) are the corresponding CS-I curves multiplied by an interpolated version of the CS-II gain curve obtained from high wavelength-resolution measurements performed on the adjacent guide tube NG-4 (Ref. 18). The symbol N_g indicated in the legend refers to the number of removable guides inserted in the beam. For $N_g=8$, the source aperture diameter is 5 cm and for $N_g=0$ the source aperture diameter is 3.8 cm. Note that the plotted point density at longer wavelengths has been reduced compared with the original simulation data in order to better distinguish the plot symbols.

estimated uncertainties in the gold foil dimensions used for this measurement). In light of the good agreement of these values, this model of the prefilter section guide was retained for all simulations.

The beryllium–bismuth crystal filter was assumed to be close to the boiling point of liquid nitrogen at atmospheric pressure (approximately 80 K). The model crystal filter transmission is derived from an average of several cross sections available from the National Nuclear Data Center[16] including data specific to 600 μm grain size beryllium and to single crystal bismuth. The separate and combined transmissions of the 8 in. Be and 8 in. Bi filter blocks at 80 K calculated from these cross-section data are shown in Fig. 7.

Since the OF was installed simultaneously with the increased brightness and nonspherical second-generation "Advanced liquid hydrogen cold source" (CS-II),[17,18] no measured data are available for the optical filter with CS-I. However, initial simulations of the OF were performed assuming the CS-I brightness and geometry in order to compare the performance of the two guides under identical illumination conditions. For the OF simulations, the same natural Ni reflectivity model was assumed for its side coatings as for the CF section. The supermirror model shown in Fig. 6 is revised over the model used in the original design study of the OF since it appears that the delivered product has an appreciably larger critical angle but lower plateau (low Q) reflectivity than was originally requested. This model was developed in order to explain the measured performance of the OF with CS-II.

The simulations produced differential neutron beam current densities, $d\varphi/d\lambda$, within the defined sample region at the sample plane. These values are shown in Fig. 8 for both the CF and OF configurations of the guide for the cases where all 8 removable guides are inserted ($N_g=8$) or all removed ($N_g=0$). For these respective cases, source apertures of diameter 5 cm and 3.8 cm were assumed to be inserted at the positions indicated in Figs. 1 and 2, corresponding to the measurement configurations of the instrument. Figure 8 shows two additional curves for the OF labeled "corrected CS-II." These are the simulated CS-I values of $d\varphi/d\lambda$ for the OF multiplied by the CS-II/CS-I cold source intensity gain factors as a function of wavelength. The CS-II cold source gain, measured at appropriately high wavelength resolution on the adjacent and similarly-illuminated guide NG-4, is shown in Ref. 18. This gain curve was interpolated to provide values for the additional simulation points that do not exist in the measurements.

The simulated "real" guide gain curve for the OF with respect to the CF arrangement, shown in Fig. 9, is evaluated as the ratio of the simulated OF to CF values of $d\varphi/d\lambda$ (shown in Fig. 8), both assuming identical CS-I illumination. It corresponds to the guide gain that would have been expected from high wavelength resolution measurements at equivalent illumination, if such measurements had been available.

However, reference measured data for both the OF and CF configurations only exist in the form of neutron current densities measured with a velocity selector operating at relatively coarse neutron wavelength resolution $[\Delta\lambda/\lambda(\mathrm{FWHM})=15\%]$. This low wavelength resolution operation of the SANS instrument is typical but leads to a perceived guide gain factor that differs from that simulated in Fig. 9 (especially in regions where the neutron spectrum varies strongly with wavelength). The velocity selector transmission function, $T_{\mathrm{VS}}(\lambda)$, at 15% resolution (corresponding to zero axial tilt of its axis of rotation) is approximately triangular with peak transmission=0.75. Thus, in order to compare simulated and measured neutron current densities,

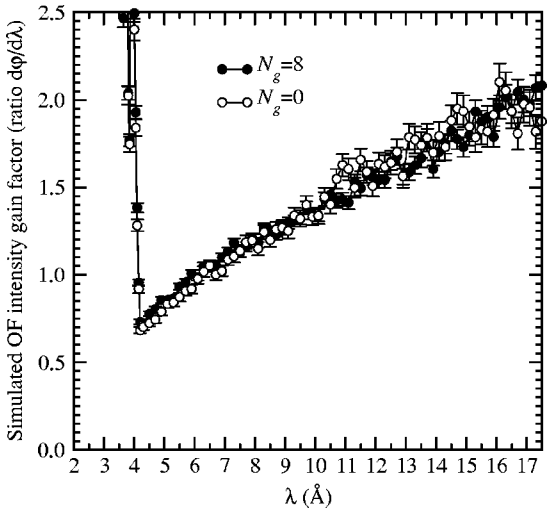

FIG. 9. Simulated "real" guide intensity gain factors of the OF (optical filter) with respect to the CF (crystal filter) guide, calculated as the ratio of the simulated differential guide fluxes $d\varphi/d\lambda$ at the same CS-I (original source) illumination. These gain factors could be compared to measurements performed at high wavelength resolution and equivalent illumination, if such measurements were available. Note that the plotted point density at longer wavelengths has been reduced compared with the original simulation data in order to better distinguish the plot symbols.

the simulated differential current densities (shown in Fig. 8) must be convoluted with $T_{VS}(\lambda_0)$ for each nominal wavelength λ_0. The resulting simulated current densities for the CF guide (CS-I illumination) are compared with the corresponding measurements in Fig. 10.

For the OF, the simulated differential current densities (assuming CS-I illumination) are first corrected for CS-II illumination, then integrated over $T_{VS}(\lambda_0)$, for each nominal wavelength λ_0 in order to obtain simulated current densities that are directly comparable with available measurements.

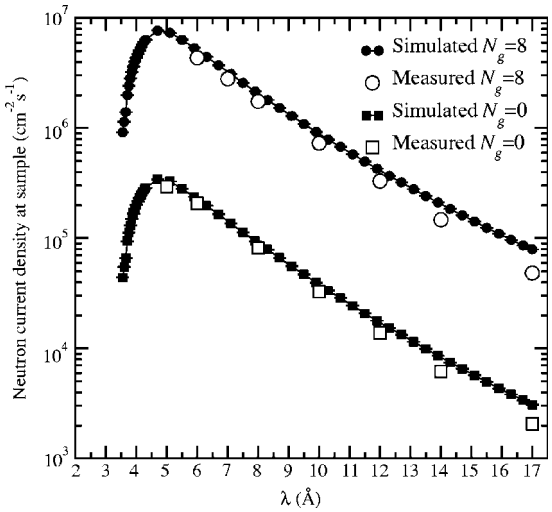

FIG. 10. Simulated and measured beam current densities, φ, for the CF (crystal filter) arrangement with the first-generation liquid hydrogen cold source (CS-I) illumination and velocity selector operation at $\Delta\lambda/\lambda(\text{FWHM})=15\%$. The simulated current densities are obtained from the simulated differential current densities by integrating over the velocity selector transmission function, $T_{VS}(\lambda_0)$, appropriate for each nominal wavelength, λ_0. Note that the plotted point density at longer wavelengths has been reduced compared with the original simulation data in order to better distinguish the plot symbols.

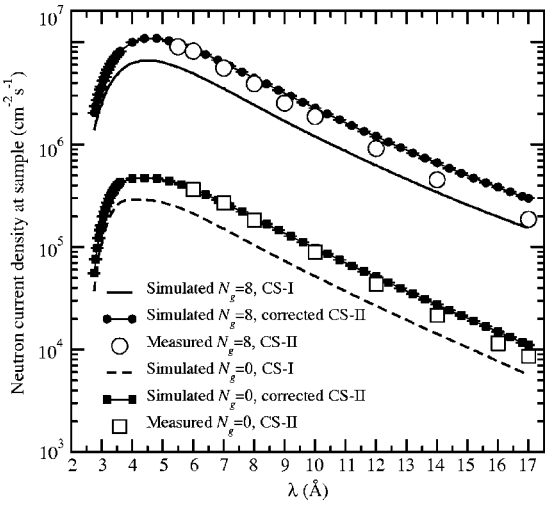

FIG. 11. Simulated and measured beam current densities, φ, for the OF (optical filter) arrangement with either 8 or 0 removable guides inserted ($N_g=8$ and $N_g=0$) for velocity selector operation at $\Delta\lambda/\lambda(\text{FWHM})=15\%$. The initial simulations of $d\varphi/d\lambda$ assuming CS-I (original source) illumination are first corrected for CS-II (upgraded source) illumination using the CS-II cold source gain factors (derived from the interpolated NG-4 data), then integrated over $T_{VS}(\lambda)$. The resulting CS-II-corrected simulated current densities are compared with the corresponding measured beam current densities for the OF with CS-II illumination. For reference, the CS-I simulated current densities are also shown. Note that the plotted point density of the simulated data at longer wavelengths has been reduced compared with the original simulation data in order to better distinguish the plot symbols.

This comparison is made in Fig. 11 (the CS-I simulation current densities obtained by eliminating the CS-II correction step are also included for reference).

The simulated "perceived" total intensity gain resulting from the combined effects of the OF and CS-II gain factors is also a quantity that is directly comparable with available measurements. This is defined as the ratio of the simulated current density at a resolution of $\Delta\lambda/\lambda(\text{FWHM})=15\%$ for the OF with CS-II (shown in Fig. 11) with respect to the corresponding value for the CF guide with CS-I (shown in Fig. 10). The measured total intensity gains are just the ratios of the measured OF and CF beam current densities [at the same resolution of $\Delta\lambda/\lambda(\text{FWHM})=15\%$]. These simulated and measured intensity gains are compared in Fig. 12.

Finally, it is interesting to compare the hypothetical real guide gain of the OF with respect to a geometry equivalent to the CF geometry but with the crystal filter and associated guide cut removed (which we call the NCF configuration). We obtain the "real" guide gain factor by taking the ratio of the simulated $d\varphi/d\lambda$ values at equivalent illumination, as before. The results are shown in Fig. 13 for $N_g=8$.

IV. DISCUSSION

In order to determine the gain of the OF relative to the CF as a function of wavelength, we need to understand the various factors that determine the transmitted intensity for each system. For the CF, there is an abrupt change in height of the guide, a factor of 6/15. The crystal transmission is negligible below $\lambda=4$ Å, rises abruptly and then decreases monotonically for large λ. There are also losses due to the guide cuts for both the filter and the velocity selector. For the

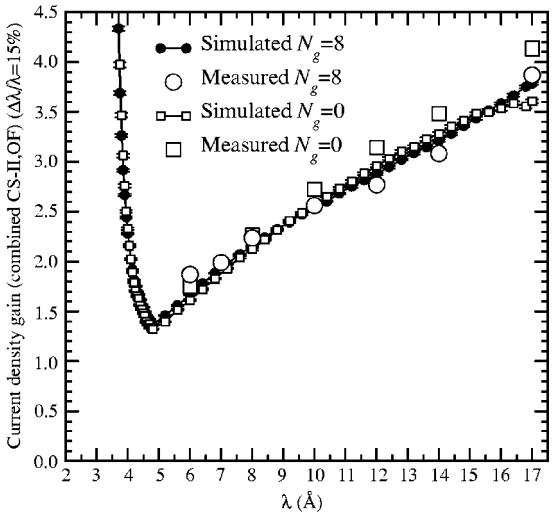

FIG. 12. Simulated and measured "perceived" current density gain factors (ratios of φ) resulting from the combined gains of the OF (optical filter) and the CS-II (upgraded cold source). The simulated gain factors were obtained by assuming the same wavelength resolution $[\Delta\lambda/\lambda(\mathrm{FWHM})=15\%]$ as the measurements. Note that the plotted point density of the simulated data at longer wavelengths has been reduced compared with the original simulation data in order to better distinguish the plot symbols.

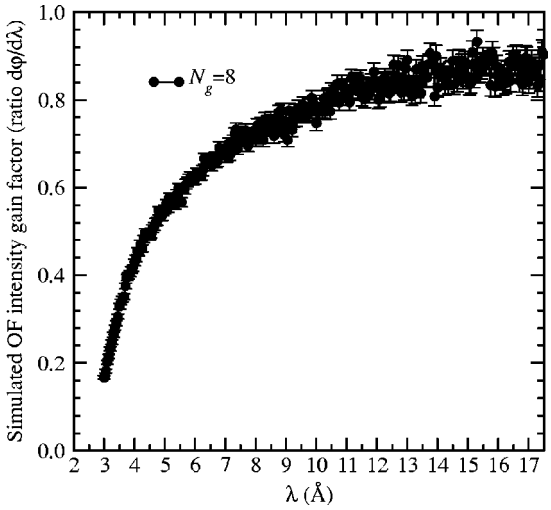

FIG. 13. Simulated OF (optical filter) gain factor (ratio of $d\varphi/d\lambda$ at equivalent illumination) with respect to the hypothetical NCF (crystal filter replaced by guide) geometry.

OF, only neutrons that undergo an even number of reflections from the parallel upward-sloping surfaces of the bend can be transmitted and enter the OF with appropriate position and angle. This factor is less than 0.5. The transmission factor of the bend itself is zero below a cutoff wavelength and increases gradually to an asymptotic value at longer wavelength. By using an OF with supermirror coatings that have critical angles about three times that of natural nickel ($m=3$), we are able to extend the SANS instrument operating range to wavelengths shorter than 4 Å. These factors explain the shape of the intensity gain as a function of wavelength shown in Fig. 9, with large gains for $\lambda<4$ Å, gains of less than unity around $\lambda=4$ Å, and the monotonically increasing gains at longer wavelengths.

Figures 10–12 demonstrate that the performance of the optical filter is quite adequately explained by the Monte Carlo models. The latter have also been used to make predictions where measured data are unavailable. We have shown that the OF successfully reaches its goals of providing both an improved and monotonically-increasing transmission over the CF with increasing wavelength from about 6 Å up, and useful intensity at nominal incident wavelengths down to 3 Å or below (having been restricted to 4 Å by the beryllium filter previously). These gains have been achieved with negligible change in the beam divergence at the sample. For long wavelength operation of the SANS instrument around $\lambda=15$ Å, the simulations indicate that the OF guide gain is around 1.8, increasing further at longer wavelength. The combined intensity gains of the OF and CS-II at $\lambda=15$ Å are by about a factor 3.4.

Judging by the measurements, the Monte Carlo models tend to slightly overpredict the beam current densities at the sample, especially at longer wavelengths. The CS-I brightness model, that was developed based on time-of-flight measurements on a neighboring guide NG-1, has been used successfully to predict integral beam current densities on other guides systems. However, the model still depends on assumptions made about the average reflectivities of the reference guide tube NG-1 and is therefore subject to some degree of systematic error. Also instrumental misalignments, that must exist to some degree, have not been taken into account in the calculations. Comparison of beam current density measurements and simulations at the shortest wavelengths suggested that the supermirror critical edge must extend well beyond the requested 3 times natural nickel ($m=3$). A model corresponding to $m\approx3.7$ (shown in Fig. 6) was necessary to reduce the cut-off wavelength to a point where agreement with the data could be achieved, but this agreement was obtained with a much poorer-than-expected low-Q reflectivity. The extended critical angle, but not the absolute reflectivity, has since been confirmed by the OF manufacturers.

The simulated and measured "perceived" intensity gains (shown in Fig. 12) are in good agreement. Any systematic errors associated with the determination of absolute intensities in the simulations might be expected to cancel to some extent, since the quantity depends on a ratio of intensities. However, the long-wavelength downturn of the simulated gain factor for $N_g=0$ does not seem to be reproduced in the measured data. This is as yet unexplained.

The gain factor of the OF with respect to the NCF, shown in Fig. 13 for $N_g=8$, indicates that the long wavelength intensity of the OF, where the presence of the bend has little detrimental influence over the overall guide transmission, is comparable to that of the NCF. Because the illumination conditions and the beam entrance and exit dimensions of the OF and NCF are identical, and the exiting beam divergence is approximately the same (as required), Liouville's theorem dictates that the performance of the OF cannot exceed that of the NCF, at least for "perfect" reflectivity. We conclude, therefore, that the OF has near-optimal performance at long wavelength.

Finally, we estimate the lifetime of the OF from a neutron radiological point of view, in particular that of the lower

sloping surface of the OF that is most exposed to the neutron flux. To a good approximation, with CS-II about 3×10^{10} thermal neutrons per second are absorbed in the boron of the glass substrate over an area of approximately 3000 cm^2, corresponding to a surface flux of approximately 10^7 cm^{-2} s^{-1}. Experience has shown that the most critical failure mode of this type of glass is due to build up of helium gas pressure within the glass caused by α-decays following neutron absorption. Problems are known to occur only at thermal neutron fluences greater than about 10^{18} neutrons cm^{-2}. Thus, the lifetime of the glass at these exposure levels is not a critical issue (about 3000 years).

ACKNOWLEDGMENTS

The authors are grateful to the National Science Foundation for financial support under Agreement No. DMR-0086210. The authors express their sincere gratitude to the NIST staff who were involved in this project; in particular, George Baltic, Don Pierce, Mike Rinehart, and Jim Moyer. The authors are indebted to David Mildner, John Copley, and Mike Rowe for valuable discussions.

[1] H. Maier-Leibnitz and T. Springer, Annu. Rev. Nucl. Sci. **16**, 207 (1966).
[2] C. J. Glinka, J. M. Rowe, and J. G. LaRock, J. Appl. Crystallogr. **19**, 427 (1986).
[3] B. M. Rustad, J. Als-Nielsen, A. Bahnsen, C. J. Christensen, and A. Nielsen, Rev. Sci. Instrum. **36**, 48 (1965).
[4] S. Holmryd and D. Connor, Rev. Sci. Instrum. **40**, 49 (1969).
[5] A. K. Freund, Nucl. Instrum. Methods Phys. Res. **213**, 495 (1983).
[6] L. A. De Graaf, Interuniversitair Reactor Institut, Delft, Report No. IRI 132-82-02 (1984).
[7] J. B. Hayter, Proc. SPIE **1738**, 2 (1992).
[8] J. R. D. Copley and J. C. Cook, Chem. Phys. **292**, 477 (2003).
[9] J. R. D. Copley, J. Neutron Res. **2**, 95 (1994).
[10] J. M. Carpenter and D. F. R. Mildner, Nucl. Instrum. Methods Phys. Res. **196**, 341 (1982).
[11] I. S. Anderson, Proc. SPIE **983**, 84 (1988).
[12] D. F. R. Mildner, Nucl. Instrum. Methods Phys. Res. A **290**, 189 (1990).
[13] D. F. R. Mildner, Nucl. Instrum. Methods Phys. Res. A **292**, 693 (1990).
[14] J. R. D. Copley, J. Neutron Res. **1**, 21 (1993).
[15] R. Lindstrom, gold foil activation measurements (NCNR) (unpublished).
[16] http://www.nndc.bnl.gov/index.jsp
[17] R. E. Williams and J. M. Rowe, Physica B **311**, 117 (2002).
[18] NIST Special Publication 993 "NCNR 2002," ed. R. L. Cappelletti (2002).